MEDICAL ROBOTS

Soft erythrocyte-based bacterial microswimmers for cargo delivery

Yunus Alapan,[1]* Oncay Yasa,[1]* Oliver Schauer,[2] Joshua Giltinan,[1] Ahmet F. Tabak,[1] Victor Sourjik,[2] Metin Sitti[1†]

Bacteria-propelled biohybrid microswimmers have recently shown to be able to actively transport and deliver cargos encapsulated into their synthetic constructs to specific regions locally. However, usage of synthetic materials as cargo carriers can result in inferior performance in load-carrying efficiency, biocompatibility, and biodegradability, impeding clinical translation of biohybrid microswimmers. Here, we report construction and external guidance of bacteria-driven microswimmers using red blood cells (RBCs; erythrocytes) as autologous cargo carriers for active and guided drug delivery. Multifunctional biohybrid microswimmers were fabricated by attachment of RBCs [loaded with anticancer doxorubicin drug molecules and superparamagnetic iron oxide nanoparticles (SPIONs)] to bioengineered motile bacteria, *Escherichia coli* MG1655, via biotin-avidin-biotin binding complex. Autonomous and on-board propulsion of biohybrid microswimmers was provided by bacteria, and their external magnetic guidance was enabled by SPIONs loaded into the RBCs. Furthermore, bacteria-driven RBC microswimmers displayed preserved deformability and attachment stability even after squeezing in microchannels smaller than their sizes, as in the case of bare RBCs. In addition, an on-demand light-activated hyperthermia termination switch was engineered for RBC microswimmers to control bacteria population after operations. RBCs, as biological and autologous cargo carriers in the biohybrid microswimmers, offer notable advantages in stability, deformability, biocompatibility, and biodegradability over synthetic cargo-carrier materials. The biohybrid microswimmer design presented here transforms RBCs from passive cargo carriers into active and guidable cargo carriers toward targeted drug and other cargo delivery applications in medicine.

INTRODUCTION

Biohybrid microswimmers, which are formed by integration of biological entities with synthetic constructs or materials, have been at the forefront of minimally invasive theranostic applications for the past decade (*1*, *2*). The potential of biohybrid microswimmers to enable in vivo active cargo delivery applications lies in their autonomously functioning biological units, which provide active propulsion and environmental sensing capabilities, and also in their steerability using external magnetic or acoustic fields (*3*). Various bacterial species, mainly *Escherichia coli, Serratia marcescens*, and *Salmonella* Typhimurium, have been extensively investigated as biological units of biohybrid microswimmers for the active delivery of cargo moieties (*4*). Bacteria, and thus bacteria-driven biohybrid microswimmers, can efficiently swim using nutrients that are already present in the local microenvironment or inside the bacterial cell and are known to have a diverse sensory system, which allows their taxis-based self-guidance both in vitro and in vivo through gradients of temperature, pH, oxygen, and different attractant chemical molecules (*5*–*12*). Autonomous propulsion and sensing abilities of bacteria have been exploited for enhancing functions of the biohybrid microswimmers for their propulsion, guidance, and delivery of various cargos through their synthetic carriers, including bare or coated microbeads, liposomes, double emulsions, nanofibrous hydrogels, and electropolymerized polypyrrole microtubes (*13*–*21*). In addition, bacteria-driven microswimmers can also be externally guided and selectively brought to target sites via magnetic steering of the microsystem through either magnetic cargo unit or natural magnetotactic bacteria (*22*–*25*). Despite all the developments, translation of bacteria-driven microswimmers to clinical diagnosis and cargo delivery applications still requires design and fabrication of multifunctional cargo carriers with superior performance in payload efficiency, biocompatibility, biodegradability, in vivo stability, and deformability.

Inside the body, certain cell types, such as macrophages and red blood cells (RBCs; also named erythrocytes), are evolutionarily specialized for optimal transportation of specific molecular cargos. Among these cell types, RBCs have received substantial interest as a model carrier due to their abundance, biocompatibility, biodegradability, non-immunogenicity, inert intracellular environment, and ease of handling (*26*). To enhance their cargo transportation efficiency, RBCs lose their nucleus and organelles during maturation from an erythroid cell lineage, which renders their complete inner volume available as cargo encapsulation space and provides high deformability (*27*). Although such advantages of RBCs as physiological carriers have been exploited in many in vitro and in vivo studies to deliver various bioactive substances and contrasting agents toward sites of action, RBCs have been mainly used as passive carriers (*28*–*31*). Actuation of RBCs loaded with magnetic nanoparticles (MNPs) was previously shown using ultrasound waves, albeit a nonspecific actuation affecting not only loaded RBCs but also regular RBCs due to the asymmetric nature of the cells (*32*). To the best of our knowledge, there has been no report in the literature on bacteria-driven propulsion of cargo-loaded RBCs that can transform passive RBCs into active autonomous microswimmers with sensing and external guiding/steering capabilities.

Here, we report biohybrid microswimmers composed of bioengineered motile bacteria and RBCs loaded with a model anticancer drug [doxorubicin (DOX)] and superparamagnetic iron oxide nanoparticles (SPIONs), which provide autonomous propulsion, nontethered magnetic steering, and efficient drug encapsulation and

[1]Physical Intelligence Department, Max Planck Institute for Intelligent Systems, 70569 Stuttgart, Germany. [2]Systems and Synthetic Microbiology Department, Max Planck Institute for Terrestrial Microbiology, 35043 Marburg, Germany.
*These authors contributed equally to this work.
†Corresponding author. Email: sitti@is.mpg.de

release. Multifunctional biohybrid microswimmers (denoted as RBC microswimmers) were fabricated by first loading DOX molecules and SPIONs into RBCs, followed by the attachment of these loaded RBCs to a bioengineered *E. coli* MG1655 via biotin-avidin-biotin binding complex (Fig. 1A). The RBC microswimmers were actuated via flagella of the bacteria and externally guided through SPIONs, loaded into RBCs, using a uniform external magnetic field (20 mT). Moreover, deformability of the cargo carrier and robustness of the integration between the bacteria and RBCs, which are critical requirements for successful operation of biohybrid microswimmers even in tight physiological environments, were tested inside microfluidic channels with gaps smaller than their size. Because of the inherent deformability of RBCs and strong noncovalent conjugation chemistry between the bacteria and RBCs, RBC microswimmers displayed high stability after squeezing through the confined channels. Furthermore, an on-demand NIR-activated hyperthermia termination switch was engineered for RBC microswimmers to control bacteria population after cargo delivery operations. The biohybrid microswimmer design approach presented here takes advantage of autologous RBCs to enable a biomaterial-based cargo-carrier architecture for biocompatible, biodegradable, and multifunctional microswimmers that can be used in future in vivo medical applications.

RESULTS

Construction of the RBC microswimmers was realized by the attachment of RBCs, loaded with DOX molecules and SPIONs, to motile peritrichously flagellated bacteria through the biotin-streptavidin-biotin binding complex. To accomplish this construction, we used a genetically engineered substrain of *E. coli* MG1655 (*33*), modified to express biotin attachment peptides on the cell membrane, to nondestructively functionalize the actuator with biotin and, subsequently, streptavidin molecules (fig. S1). In parallel, cargo-loaded RBCs were prepared using hypotonic treatment and decorated with biotin molecules via specific attachment of biotin-conjugated TER-119 antibodies onto the membrane of RBCs (fig. S2). RBC microswimmers were then constructed through noncovalent interaction of biotin-functionalized RBCs with streptavidin-coated motile bacteria (Fig. 1B). Biotin-streptavidin binding complex, which is one of the strongest known noncovalent interaction in nature, was chosen for the construction of RBC microswimmers to provide robust attachment between bacteria and RBCs and to ensure stability in chemically and physically harsh conditions. Bacteria were observed to preserve their attachment with the cargo when they were integrated with DOX-loaded RBCs (fig. S3), and they were also able to propel the payload with ease through the solution (Fig. 1C and movie S1).

Encapsulation of DOX and SPIONs into the RBCs was realized using a sequential hypotonic isotonic treatment process (Fig. 2A). Briefly, RBCs were incubated in a gently shaking hypotonic solution along with DOX and 50-nm citric acid–coated SPIONs at 4°C. Incubation of RBCs in a hypotonic solution causes swelling of the cells and formation of about 100-nm-diameter pores on the cell membrane, which results in outward diffusion of hemoglobin content and inward diffusion of DOX molecules and SPIONs (*34*). Once the diffusion equilibrium was reached, RBCs were centrifuged and transferred into an isotonic solution at 37°C to reseal their cell membrane—and, thus, to entrap DOX and SPIONs. This process resulted in efficient loading of drug molecules and SPIONs while preserving critical membrane

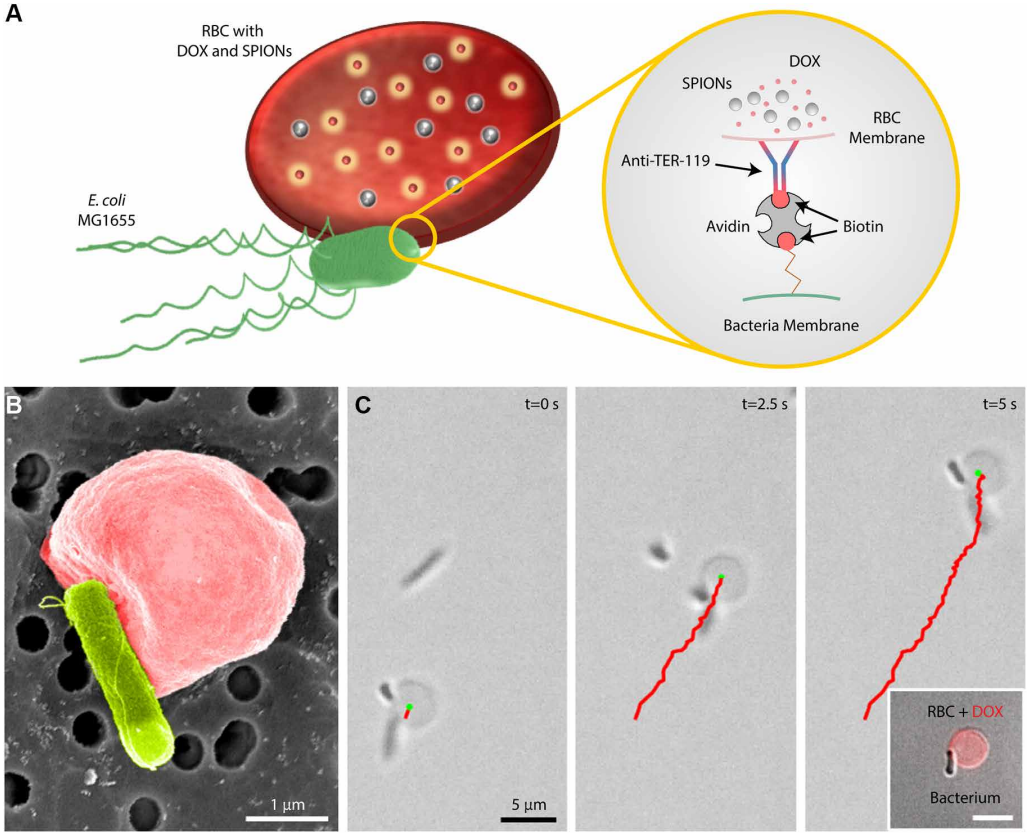

Fig. 1. RBC microswimmers for active cargo delivery. (**A**) RBC microswimmers are composed of an RBC, loaded with drug molecules and SPIONs, bound to a motile bacterium (bioengineered *E. coli* MG1655) via biotin-avidin-biotin binding complex. (**B**) SEM image (pseudocolored red, RBC; pseudocolored green, bacterium) of an example RBC microswimmer with an attached bacterium. (**C**) Example 2D propulsion trajectories of RBC microswimmers over time. The inset displays a bacterium attached to an RBC loaded with DOX molecules. Scale bar, 5 μm.

properties of the RBCs, including membrane target ligand (TER-119) used to bind biotin-conjugated antibodies (Fig. 2B and figs. S2 and S4). Flow cytometry analyses demonstrated that RBCs preserved their membrane ligands after the sequential hypotonic-isotonic treatment (Fig. 2C and figs. S5 and S6). Before the treatment, 78.11% of the RBC population was TER-119–positive, and the treatment process did not alter the percentage of TER-119–positive cells (77.97% of the RBC population). The flow cytometry results also showed that 78.37% of the RBC population successfully encapsulated DOX, and overall, 54.52% of the RBC population was double-positive for both DOX and TER-119 (Fig. 2C). Encapsulation efficiency of DOX in RBC cargoes was around 78%. Release of DOX molecules from RBC cargoes was analyzed over 120 hours at different pH conditions, ranging from 3.1 to 9.2, to evaluate pH responsiveness (Fig. 2D). The results showed an enhanced release of DOX at lower pH values, especially at pH = 3.1. Within 24 hours, around 98% of the drug molecules were released at 3.1, whereas less than 70% were released at pH = 7.2. Moreover, a burst release was observed within 3 hours, with around 70% release at pH = 3.1 and more than 40% release at pH = 7.2. However, drug release was continued almost at a constant rate until 96 hours at pH = 7.2. These results show a pH-dependent release rate, with considerably enhanced release rates at lower pH values, most likely due to swelling of RBCs osmotically and their eventual hemolysis (*35*). Such enhanced release at low pH may be especially useful for applications aimed at cargo delivery to cancer cells, which flourish in a highly acidic tumor microenvironment (*36*). Furthermore, RBCs loaded with SPIONs displayed attraction to a permanent magnet, providing qualitative information about the magnetic properties of the RBCs after the hypotonic-isotonic treatment process (fig. S7). Entrapment of SPIONs in RBCs was further confirmed with energy-dispersive x-ray spectroscopy (EDS) analysis (fig. S8).

After fabrication of RBC microswimmers via attachment of bioengineered bacteria and RBCs through biotin-avidin-biotin binding complex, motility characteristics of the microsystem, including average velocity and two-dimensional (2D) swimming trajectories, were analyzed and

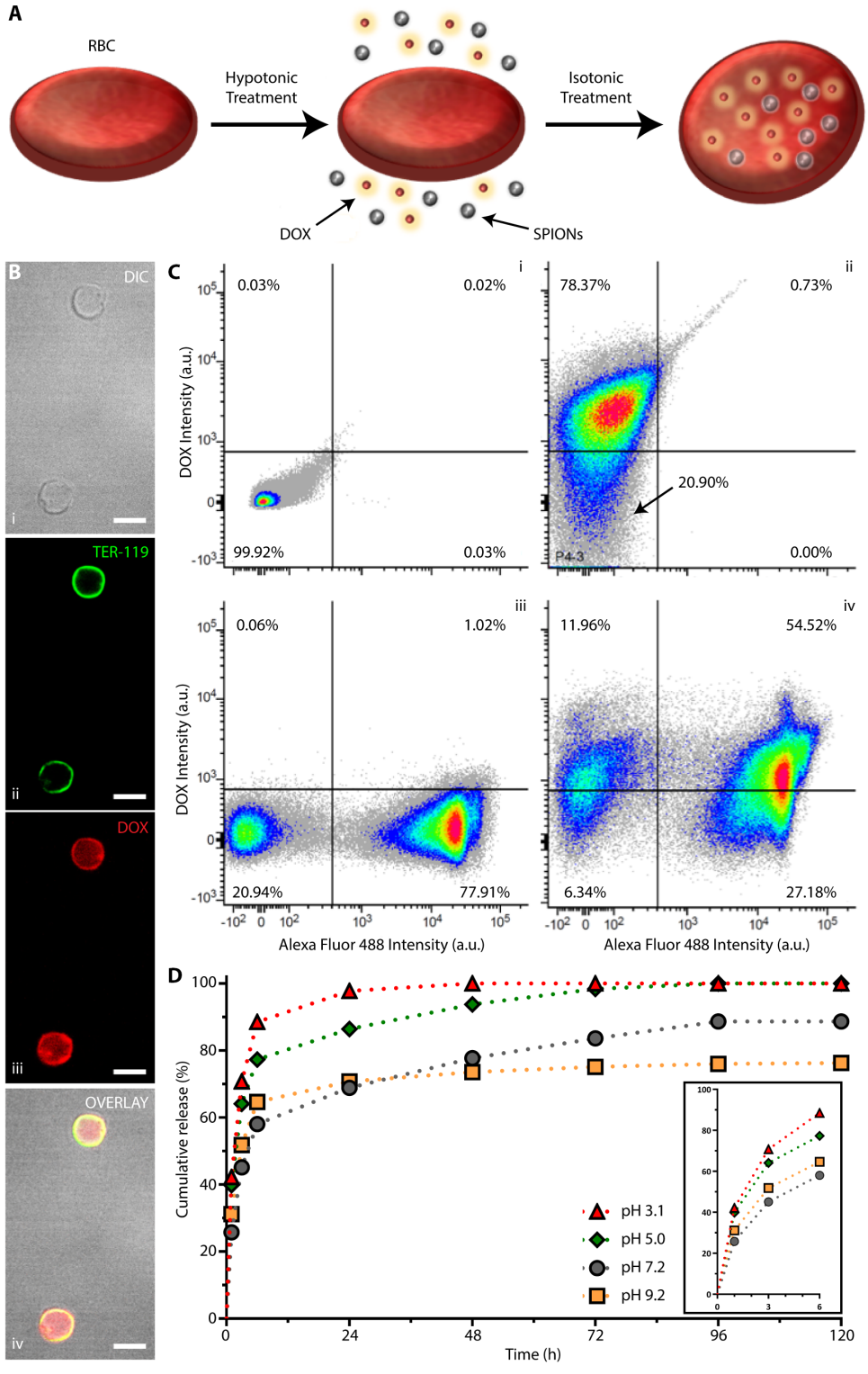

Fig. 2. RBC microswimmers loaded with DOX molecules preserve their membrane proteins after hypotonic treatment. (**A**) Loading of DOX molecules and SPIONs is achieved via hypotonic dilution technique. (**B**) RBCs (i) loaded with DOX via hypotonic dilution method (ii) preserve their membrane expression of TER-119 (iii and iv). DIC, differential interference contrast. (**C**) Flow cytometry density plots obtained from RBCs (i) after hypotonic-isotonic treatment, (ii) DOX encapsulation, (iii) anti–TER-119 staining, and (iv) both anti–TER-119 staining and DOX encapsulation show successful encapsulation of DOX and TER-119 expression. a.u., arbitrary units. (**D**) Cumulative released percentage of DOX molecules over time (5 days) from RBC cargoes at pH = 3.1, 5.0, 7.2, and 9.2.

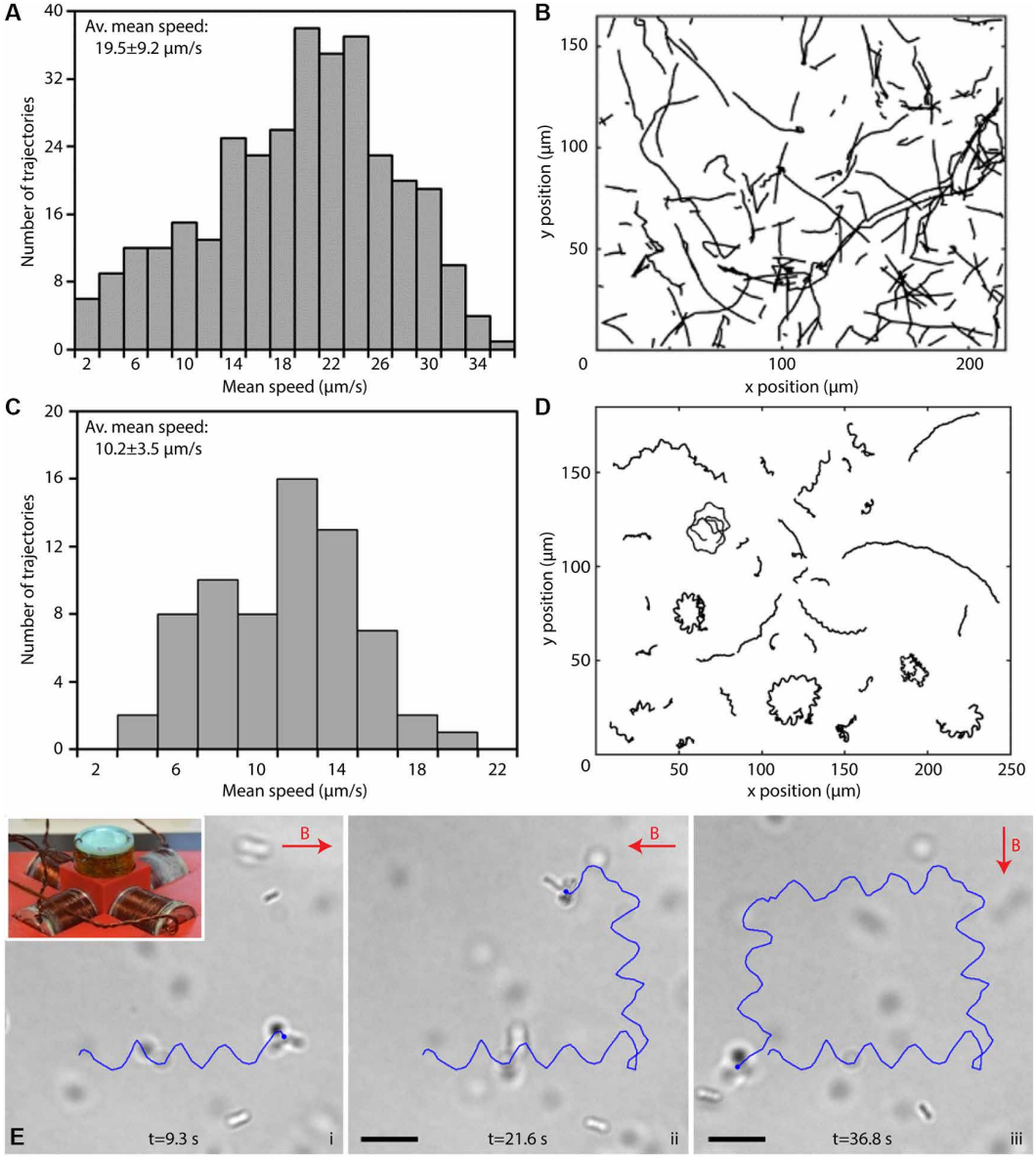

Fig. 3. 2D motility characterization and external magnetic steering of RBC microswimmers. (**A** to **D**) Mean speed distribution and 2D swimming trajectories of (A and B) free bacteria and (C and D) bacteria-driven RBC microswimmers, respectively. Free bacteria displayed a mean speed of 19.5 ± 9.2 μm s^{-1}, whereas the mean speed of RBC microswimmers was 10.2 ± 3.5 μm s^{-1}. (**E**) Magnetic steering of an RBC microswimmer and change in swimming direction upon change in magnetic field direction (i to iii). Red arrows indicate the direction of the magnetic field (***B***). The inset shows the five-coil setup used for magnetic steering of the RBC microswimmers. Scale bars, 10 μm.

compared with free swimming bacteria (Fig. 3, A to D). The measured average velocity of freely swimming bioengineered *E. coli* MG1655 was 19.5 ± 9.2 μm s^{-1}, which is comparable with the average velocity of wild-type *E. coli* (*37*). This result shows that expression of biotin attachment peptides and subsequent functionalization on the cell membrane of bacteria had a negligible effect on motility of the bacteria. The measured average velocity of multifunctional biohybrid microswimmers was 10.2 ± 3.5 μm s^{-1}, which is relatively higher compared with the previously reported bacteria-based biohybrid microswimmers composed of similar-sized cargo units (*4*). The observed superior speed performance of the proposed RBC microswimmer might be due to the lower density (1.080 to 1.120 g ml^{-1}) and higher buoyancy of RBCs compared with synthetic carriers (*38*). Moreover, although some of the RBC microswimmers followed smoother random paths, others displayed wavy, spiral-like trajectories (Fig. 3D). This difference in swimming trajectories may have been due to random attachment of bacteria to RBCs, because attachment from the side of the cell causes an off-axis propulsion, resulting in a combined rotational and translational motion (*39*).

Encapsulation of SPIONs into the RBCs allowed external guiding of RBC microswimmers under a uniform magnetic field generated by using a custom-made electromagnetic coil setup mounted on an inverted optical microscope (Fig. 3E and fig. S9). SPION encapsulation and asymmetrical aggregation inside RBCs provide net magnetization and thus alignment along the applied magnetic field direction (*32*). Fabricated RBC microswimmers were injected into a microchannel, which was then placed inside the five-coil electromagnetic setup for the steering of microswimmers. RBC microswimmers displayed swimming paths parallel to the applied magnetic field (20 mT), whereas RBCs without any attached bacteria did not display any net displacement, indicating the necessity of an on-board actuator for guided swimming of the RBCs. Controlled guidance of RBC microswimmers was realized under uniform magnetic fields, demonstrating a square swimming path (Fig. 3E and movie S2).

Inside the body, motility and transportation of certain cell types occur through deformation and adaptation of the cells to tissue microenvironment. Therefore, the ability to deform and pass through confined spaces without damaging the carrier, cargo, and propeller is a critical prerequisite for all microswimmer designs intended for in vivo operation. To investigate deformability of the proposed RBC microswimmers and stability of their components, we injected and squeezed them through microfluidic channels with a width of 3 μm, which is smaller than the size of the RBCs (4 to 5 μm). RBC microswimmers were able to deform inside the microchannels and pass through with ease (Fig. 4A, figs. S10 and S11, and movie S3). Moreover, the RBC microswimmers preserved their integrity when deformed inside the microchannels and collected at the outlet (Fig. 4, B and C). The percentage of RBC microswimmers before injection (fabrication yield, ~72% of the total RBC population) did not decrease significantly (two-tailed *t* test, $P > 0.05$) after squeezing through the microchannels (~50%) (Fig. 4D), demonstrating the stability of the microswimmers and their future potential for in vivo applications. Of note, a comparison of initial RBC microswimmer fabrication yield (~72%) with TER-119–positive RBC population (77.91%), measured in flow cytometry analyses, also indicated an effective microswimmer fabrication efficiency of more than 90%. Furthermore, active deformation and passage of RBC microswimmers through confined spaces smaller than their size only by means of bacterial propulsion were investigated (Fig. 5 and movie S4). Microgaps inside a microfluidic channel were formed by fabrication of circular micropillars with a controlled gap distance of 2 μm. Then, RBC microswimmers were injected into the microfluidic channel with pillar array and sealed completely to prevent fluid drift. Within the microchannels, an RBC microswimmer was observed to approach and deform its cargo unit between the gap smaller than its size actively by propulsion of its bacterium unit. During and after deformation and passing through the microgap, the RBC microswimmer was able to preserve its integrity, as well as motility. This observation demonstrated the proof of concept that bacteria can generate enough force to deform its carrier through a narrow gap and pass through. The deformability of the RBC microswimmers is due to the inherent flexibility of RBCs, whereas the stability of attachment is due to the strong noncovalent interaction between biotin and avidin molecules, which couples bacteria and RBCs.

Biohybrid microswimmers, especially the ones driven by microorganisms such as bacteria, provide considerable advantages compared with their synthetic counterparts, including dynamic response to changing environmental conditions and use of inexpensive and eco-friendly fuel. However, one caveat of using microorganisms in biohybrid

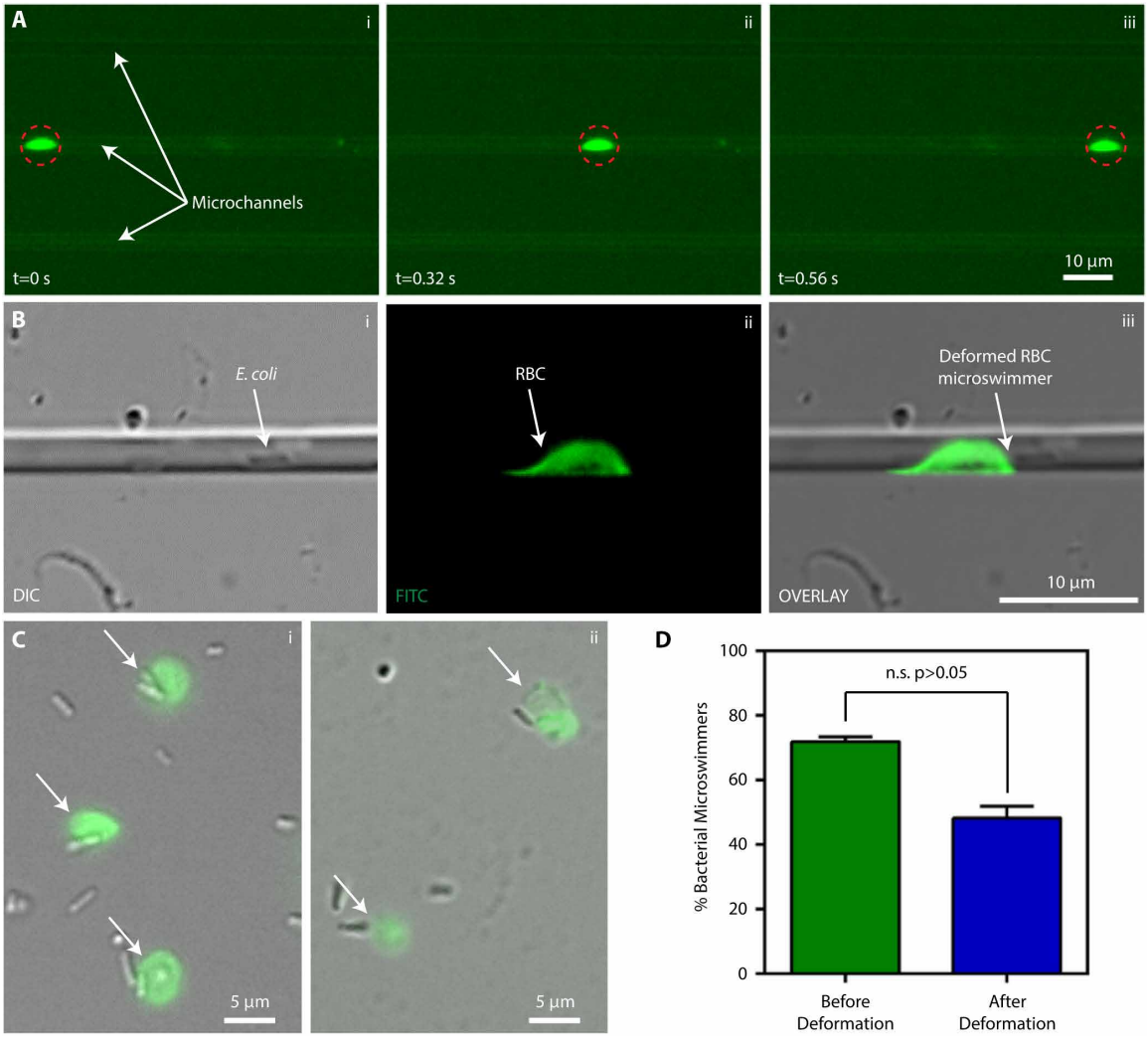

Fig. 4. Deformability and stability of RBC microswimmers squeezing through confined spaces smaller than their size. (**A**) RBC microswimmers, fluorescently labeled, were able to squeeze with ease through microchannels with a width of 3 μm, which is smaller than the size of RBCs (4 to 6 μm). RBCs moving through a single channel over a time period of 0.56 s (i to iii) were highlighted with red circles. (**B** and **C**) RBC microswimmers preserved their integrity when (B) deformed inside the microchannels and (C) collected at the outlet. White arrows indicate intact RBC microswimmers, where bacteria preserved their attachment to RBCs. (**D**) Change in percentage of RBC microswimmers after squeezing through microfluidic channels was not statistically significant (Mann-Whitney test, $P > 0.05$). Error bars represent the SD. n.s., not significant.

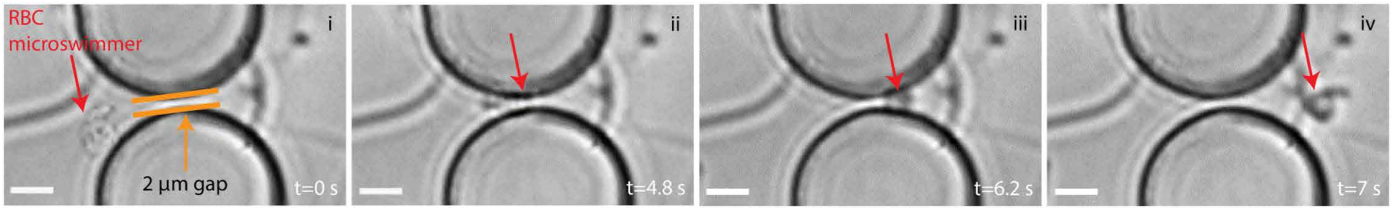

Fig. 5. Active deformation of an RBC cargo propelled and pushed by a single bacterium through a 2-μm gap. RBC microswimmer approaches to a gap formed by two adjacent micropillars (i), bacterium pushes the RBC to deform within the microgap (ii and iii), and the RBC microswimmer moves out of the microgap while preserving its stability and motility (iv). Scale bars, 5 μm.

microswimmer designs is rapid and uncontrolled proliferation of microorganisms (e.g., ~20 min of doubling time in case of *E. coli*). Therefore, a termination switch is required in ideal biohybrid microswimmer designs to stop uncontrolled growth of microorganisms and prevent any potential side effects. We engineered an on-demand hyperthermia termination switch activated via NIR to control bacteria population in RBC microswimmer samples (Fig. 6). To realize NIR-activated termination, we coupled indocyanine green (ICG), a NIR photothermal agent, to bovine serum albumin (BSA) and loaded it into RBCs (Fig. 6A). Upon irradiation with NIR light, adsorbed energy is converted to heat inside the molecule, resulting in hyperthermia (>60°C of maximum temperature; Fig. 6B) along with rupture of RBC membrane and death of attached bacteria (Fig. 6C). The number of intact RBCs was significantly lower in samples irradiated with NIR and underwent hyperthermia than in those before irradiation (Fig. 6D). Furthermore, the percentage of viable bacteria decreased significantly in samples irradiated with NIR (~16%) compared with those without any irradiation (~82%; Fig. 6E). Using ICG-BSA–loaded RBCs, we have shown the proof of concept of on-demand, NIR-triggered termination of bacterial microswimmers, providing a feasible and noninvasive means of controlling bacteria population of biohybrid microswimmers.

DISCUSSION

In nature, various cell types are specialized in delivery of substances by leveraging their unique features, including deformability, target affinity, taxis, and barrier-crossing capability. Such unique features of natural cells—including RBCs, stem cells, T lymphocytes, and macrophages—have been used in systemic delivery of drugs and various imaging agents (*26*, *40*). RBCs are the natural carriers of the body, constituting more than 90% of the blood cells. Because of their abundancy and affordability, RBCs represent the most feasible, high-throughput, and practically applicable personalized carrier for cargo delivery (*26*). Moreover, RBCs are uniquely specialized to carry maximum loads by losing their nuclei through maturation, which also allows them to deform and squeeze repeatedly without blocking any capillaries that can be as small as half of their diameter (*41*–*43*). Because of such unique capabilities, RBCs have been used intensively as passive carriers for delivery of drugs targeting several maladies—such as oncologic, inflammatory, and neurological diseases—and as imaging agents for diagnostic applications (*26*, *44*, *45*).

Despite such vast utilization of RBCs as passive carriers in cargo delivery, engineering RBCs as microswimmers for active propulsion is still an open area for investigation. Actuation of RBCs was shown previously by means of beating magnetic filaments under oscillating fields, as well as acoustic propulsion of MNP-loaded RBCs. In 2005, Dreyfus *et al.* (*46*) described propulsion of RBCs using a linear chain of colloidal magnetic particles linked by DNA, which was actuated under an oscillating magnetic field. Although this study demonstrated the controlled propulsion of RBCs with an oscillating magnetic field as a proof of concept, the described approach suffers from a complex and expensive fabrication process, which limits its potential biomedical applications. Moreover, Wu *et al.* (*32*) developed a hybrid micromotor by loading citrate-stabilized MNPs into RBCs to actuate and control the motion with ultrasound and external magnetic field, respectively. Later, co-encapsulation of quantum dots and drug molecules with MNPs into RBCs was also demonstrated, and their actuation and steering inside a complex microchannel were investigated (*47*). Although the use of ultrasound provides external actuation, asymmetric shape of RBCs leads to actuation of not only RBC micromotors but also regular RBCs. The RBC microswimmer approach presented here transforms passive RBCs into active soft microswimmers with autonomous, onboard actuation and sensing capabilities, via motile bacteria, and external guiding, via SPIONs encapsulated in RBCs.

The biohybrid microswimmer design approach presented here yielded higher fabrication efficiency, speed, and deformability compared with previously reported bacteria-driven microswimmers using *E. coli* as the propeller but carrying a synthetic cargo unit. As previously shown, the mechanical properties of the cargo unit, especially softness, have direct effect on optimum attachment of bacteria to the cargo surface, which may also have been in effect for the high yield of RBC microswimmer fabrication reported here (*16*). Moreover, the density of RBCs is inherently lower than synthetic materials and provides buoyancy to the fabricated RBC microswimmers. Aside from *E. coli*, other bacteria species with higher swimming speeds [e.g., ~30 μm s^{-1} for *S. marcescens* (*48*) and ~100 μm/s for *Magnetococcus marinus* strain MC-1 (*17*)] have been previously used as bioactuators for microswimmers. Despite its relatively lower speed compared with other bacteria, we specifically used *E. coli* because of its well-understood genetics, which allowed us to engineer biotin attachment peptide on its membrane. By using this peptide, we were able to fabricate RBC microswimmers through biotin-avidin interaction, which eliminated the need for harsh chemical reactions [e.g., 1-ethyl-3-(3-dimethylaminopropyl)-carbodiimide-N-hydroxysuccinimide (EDC-NHS)] that were heavily used in previously reported bacteria-based microswimmers. When abovementioned properties were considered together, the RBC microswimmers presented here displayed higher average velocities compared with previous designs using synthetic cargo carriers and chemical attachment methods (*4*). Last, inherent flexibility of RBCs provides a valuable asset to the RBC microswimmers presented here in terms of deformability, which might prove to be a critical advantage in in vivo cargo delivery applications.

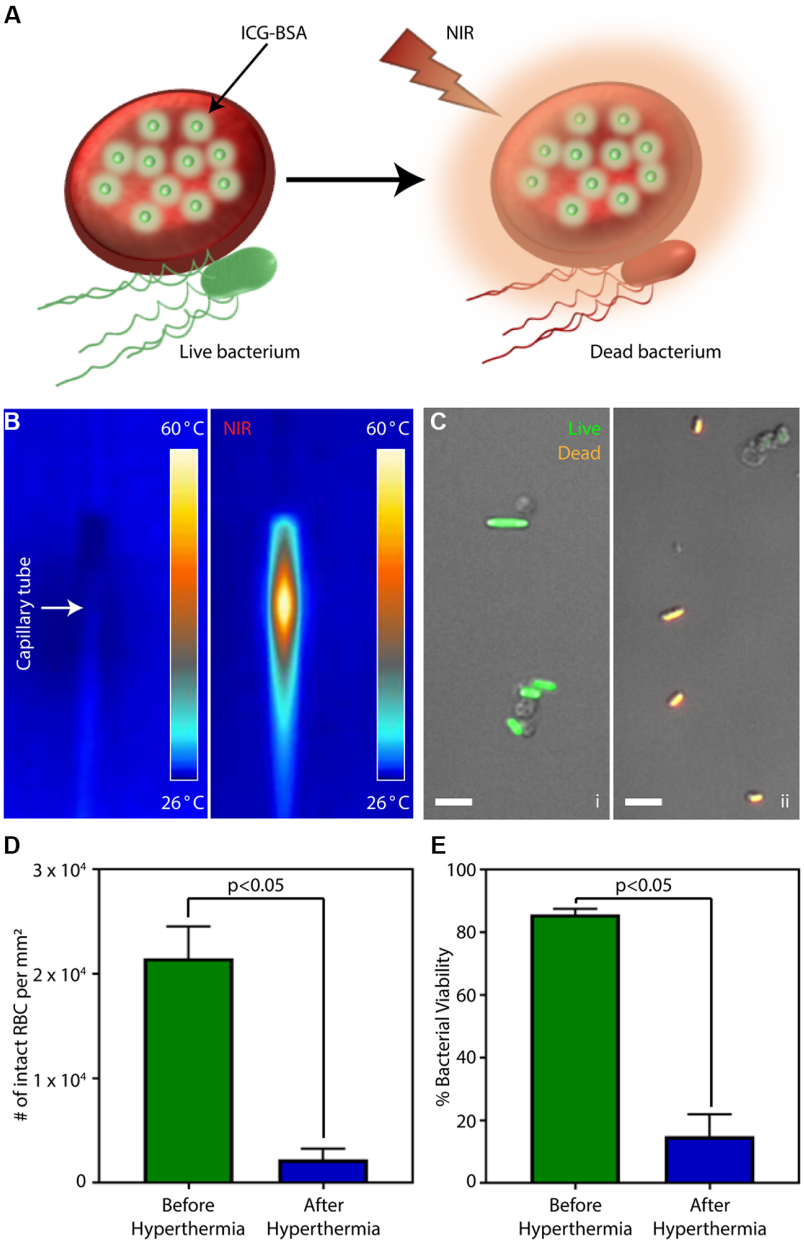

Fig. 6. On-demand, NIR light–triggered hyperthermia termination switch for RBC microswimmers. (**A**) Schematic RBC microswimmers, loaded with a photothermal agent (ICG) coupled with BSA, generating heat upon irradiation with NIR and resulting in termination of bacteria. (**B**) IR thermal images of RBC microswimmers loaded inside a capillary tube before and during NIR irradiation. (**C**) Live/dead staining of bacteria in RBC microswimmer samples before (i) and after (ii) NIR irradiation, respectively. Scale bars, 5 μm. (**D** and **E**) Quantitative measurements of (D) number of intact RBCs and (E) percent viable bacteria before and after NIR-activated hyperthermia termination, respectively. Error bars represent the SD.

RBCs, as nature's own carriers, have been extensively investigated as non–genetically engineered cargo carriers for theranostic applications. Although ex vivo engineered RBCs showed better biocompatibility and immune-evasive properties compared with synthetic systems, including conventional liposomal delivery platforms, there are still major challenges that need to be addressed before their full translation into the clinic (*26*, *49*). Specifically, in microswimmer applications, fabrication of biohybrid designs involving RBCs needs to be critically optimized to minimize membrane damage to the RBC and to avoid excessive cross-linking, which might compromise biocompatibility and lead to rapid clearance in vivo (*26*). For example, nonspecific chemical reactions used for coupling peptide sequences or drugs onto RBC membrane may inhibit membrane molecules—including CD47, CD59, and C8bp—that protect against phagocytosis and assembly of membrane attack complexes (*26*). Therefore, noninvasive and specific fabrication methods, such as the one used here, are needed to preserve membrane properties. Furthermore, RBCs are limited in their ability to cross biological barriers, such as the blood-brain barrier, which needs to be taken into account in targeted delivery applications of microswimmers using RBCs as cargo carriers. Last, pH-dependent release of drug molecules from RBCs may not be feasible and sensitive enough for all clinical scenarios, which would necessitate on-demand and site-specific active release mechanisms.

Termination of bacteria propulsion and other functions after delivery operations or in case of emergencies is a critical component of biohybrid microswimmer design, although it is largely neglected in the literature. We used ICG molecules, coupled with BSA, loaded inside RBCs to induce noninvasive activation of hyperthermia in RBC microswimmers to terminate bacterial functions. ICG is a water-soluble tricarbocyanine dye with a strong absorption band around 800 nm. ICG was first approved for clinical applications by the U.S. Food and Drug Administration in 1956, and today it is widely used in human medical imaging and diagnosis (*50*). Photothermal capabilities of ICG have been recently coupled to RBCs and RBC-derived vesicles for photodynamic therapy combined with active drug release (*51*, *52*). Here, we used the photothermal capability of ICG as a termination switch that can be activated remotely to stop functioning of bacteria. Although NIR light has a penetration depth of 3 to 5 mm into the skin, such a termination switch may still be useful in applications targeting subcutaneous tumors or tumors lining inner cavities, such as colon, with the assistance of an endoscopic or colonoscopic irradiation. Furthermore, hyperthermia of biohybrid microswimmers can be potentially induced using other activation means, including alternating magnetic fields or ultrasound (*53*).

RBCs have been exploited as cargo carriers because of their greater biocompatibility and immune-evasive stealth properties, especially compared with synthetic cargo carriers. In nature, specific pathogens, ranging in size from 0.2 to 2 μm (e.g., hemobartonella), can bind to RBC membrane to evade immune system and remain in circulation for weeks (*54*). Furthermore, by mimicking nature, dramatically increased retention times were also shown for polystyrene particles that are attached to (hitchhiking) RBCs compared with free particles (*54*, *55*). Drawing similarities between RBC microswimmers introduced in this report and analogs available in nature or engineered systems, our RBC microswimmers would also have better biocompatibility compared with free bacteria, which we will investigate in future work.

The RBC microswimmers reported here demonstrate a unique multifunctionality that has not been observed in other bacteria-driven microswimmers, including (i) facile, noninvasive, and high-throughput fabrication; (ii) magnetic steerability; (iii) compliant cargo that can be actively deformed via the force generated by bacteria; and (iv) an on-demand NIR light–activated hyperthermia termination switch. Although high-throughput fabrication and magnetic steering of biohybrid microswimmers have been previously shown (*1*, *12*, *16*), the RBC microswimmer design described here combines these features with additional advanced functionalities, including active deformation of the soft cargo and on-demand termination switch of the actuators, within the same platform. The presented biohybrid microswimmer demonstrates engineering and integration of one of nature's most efficient microswimmers (bacterium) and cargo carriers (RBC) to create the blueprint for the next generation of multimodal, targeted cargo delivery systems.

MATERIALS AND METHODS

Encapsulation of DOX and SPIONs in RBCs

Purified mouse RBCs were purchased from Innovative Research (Novi, MI). RBCs were washed three times with phosphate-buffered saline (PBS; pH 7.2), and 250 μl of RBCs was incubated in deionized (DI) water for 15 min. Afterward, 150 μl of SPION solution [25 mg ml^{-1}, 50 nm; chemicell (Berlin, Germany)] and 100 μl of DOX solution (500 μg ml^{-1}; Sigma-Aldrich) were mixed with the RBCs. A mixed solution of RBCs with SPIONs and DOX was incubated at 4°C for 1 hour to ensure swelling of RBCs and pore formation for diffusion of SPIONs and DOX into the RBCs. The loaded RBCs were rinsed three times with PBS at room temperature and incubated for 1 hour at 37°C for resealing the RBCs. Resealed RBCs were incubated with anti-mouse TER-119 antibody conjugated with biotin for attachment to streptavidin-conjugated bacteria.

Characterization of DOX- and SPION-loaded RBCs

Alexa Fluor 488–conjugated TER-119 antibodies (BioLegend, San Diego, CA) were used to characterize the expression of TER-119 antigen on mouse RBCs before and after drug and SPION loading. Fluorescein isothiocyanate (FITC)–conjugated streptavidin (Sigma-Aldrich) was also used to confirm binding of biotin-conjugated TER-119 antibodies to RBCs. DOX loading into RBCs was confirmed using autofluorescence of DOX (excitation, 470 nm/emission, 585 nm). Attachment of TER-119 antibodies and DOX loading into RBCs were validated using flow cytometry analyses. DOX-loaded RBCs labeled with Alexa Fluor 488–conjugated TER-119 antibodies were analyzed using a BD FACSMelody cell sorter (BD Biosciences, East Rutherford, NJ). For each experiment, 250,000 events were recorded using a 488-nm laser for excitation, and 527 ± 16–nm emission filter for Alexa Fluor 488 and 700 ± 27–nm emission filter for DOX.

Scanning electron microscopy (SEM) imaging of RBC microswimmers was performed via a Zeiss Ultra 550 Gemini scanning electron microscope (Carl Zeiss Inc., Oberkochen, Germany) using an accelerating voltage of 5 keV and an in-lens detector. For SEM imaging, RBC microswimmer samples were injected through track-etched polycarbonate membrane filters (Whatman, Maidstone, UK) with a pore diameter of 200 nm. Membrane filters were incubated in 2.5% glutaraldehyde at 4°C for 1 hour. Afterward, the samples were dehydrated in sequentially increasing ethanol concentrations up to 100% ethanol. The samples were dried using an automated critical point dryer (Leica EM CPD300, Leica Microsystems, Wetzlar, Germany) and coated with 10 nm of gold using a Leica EM ACE600 sputter coater (Leica Microsystems). EDS (Bruker, Billerica, MA) was performed to analyze loading of SPIONs into RBCs, using an accelerating voltage of 15 keV.

pH-responsive drug release

After the DOX loading process as described above, RBCs were centrifuged to collect unloaded DOX molecules in the supernatant. To characterize drug release, we suspended RBCs (500×10^6 cells) in 1 ml of medium at different pH values and incubated them at room temperature, 250 rpm. At predetermined time points, samples were centrifuged to collect supernatants and replaced with the equal volume of fresh medium. Loading and release of DOX were quantified from collected supernatants, in combination with a standard curve of DOX solutions (4 to 250 μg ml^{-1}), by measuring absorbance at 480 nm using a plate reader (BioTek Gen5 Synergy 2, Bad Friedrichshall, Germany).

Fabrication of RBC microswimmers

Bioengineered bacteria strain is derived from *E. coli* MG1655. It contains pOS233 plasmid, which was modified in antigen 43 (Ag43) region to express FLAG epitope and biotin attachment peptide (fig. S1A) (*33*). A single colony of bioengineered *E. coli* MG1655 was cultured overnight at 37°C, 200 rpm in TB medium [10 g of tryptone and 5 g of NaCl in 1 liter of distilled water (pH 7.0)] containing kanamycin (50 μg ml^{-1}; Sigma-Aldrich) and ampicillin (100 μg ml^{-1}; Sigma-Aldrich). Then, 100 μl of overnight culture was transferred into 10 ml of TB medium containing biotin (1 μM), kanamycin (50 μg ml^{-1}), and ampicillin (100 μg ml^{-1}) and cultured for 2 hours at 34°C, 270 rpm. At the end of 2 hours, 100 μM isopropyl-β-D-thiogalactopyranoside (Sigma-Aldrich) was added and further cultured in the same conditions until OD_{600} (optical density at 600 nm) (BioTek Gen5 Synergy 2 plate reader, Bad Friedrichshall, Germany) reached 0.6. After rinsing the bacteria with motility medium twice, we incubated the bacteria in motility medium [10 mM K_2HPO_4, 10 mM $KHPO_4$, 67 mM NaCl, 0.1 mM EDTA, 1% (w/v) glucose (pH 7.0)] with streptavidin (100 μg ml^{-1}; Sigma-Aldrich) at 37°C and 200 rpm for 1 hour. After the incubation, the bacteria were rinsed twice and resuspended in motility medium.

Streptavidin-conjugated bacteria were mixed with DOX- and SPION-loaded RBCs for fabrication of RBC microswimmers and incubated at room temperature for 5 min. After attachment, RBC microswimmers were injected into a microchannel (75 μm height by 2 mm width by 10 mm length), composed of laser-cut poly(methyl methacrylate) pieces and double-sided adhesive films attached to a cover glass for motility characterization (*56*).

Motility characterization and magnetic guidance of RBC microswimmers

RBC microswimmers were tracked from video recordings (30 frames per second) obtained using an inverted optical microscope with 40× water immersion objective lens (DMi8, Leica Microsystems). Motility characterization parameters including mean speed and velocity for both free bacteria and RBC microswimmers were computationally analyzed using an in-house tracking software developed in MATLAB (MathWorks, Natick, MA).

We used a custom five-coil magnetic guidance setup built on an inverted microscope (Zeiss Axio Observer A1, Carl Zeiss) housing a microfluidic channel. The magnetic guidance system was designed to generate magnetic fields up to 20 mT in *x* and *y* directions. Each coil

was controlled independently by a current controller (Escon 70/10, Maxon Motor AG), and desired current values were determined by the precalibrated field to current ratios. The field was measured to be uniform within 5 mm from the center of the workspace in the *x*-*y* plane. The *z* axis coil (out of plane) was not used in this work.

Deformability analysis of RBC microswimmers

Passive deformability and stability of the RBC microswimmers were investigated by flowing microswimmers through microchannels with a width of 3 μm, whereas active deformation of RBC microswimmers by bacterial propulsion was investigated by using a microfabricated fluidic channel incorporating circular pillar arrays with a controlled gap distance of 2 μm. Microfluidic channels were fabricated on the basis of photolithography and soft lithography (*57*, *58*). A negative template on a silicon wafer was fabricated using photolithography and silanization with (tridecafluoro-1,1,2,2-tetrahydrooctyl)-1-trichlorosilane vapor under vacuum. Then, poly(dimethylsiloxane) (PDMS; Sylgard 184, Ellsworth Adhesives, Germantown, WI) prepolymer (10:1 weight ratio, mixed and degassed) was molded over the negative template and cured at 90°C for 4 hours. After curing, the PDMS block with microchannels was peeled off, treated under oxygen plasma, and bonded to a precleaned cover glass. Inlet ports were opened using a biopsy punch (0.75 mm diameter), and rectangle outlet ports were cut open using a razor blade. Once the channels were ready, fluorescently labeled RBC microswimmers were manually injected through the microchannels using a syringe and inlet tubing.

NIR-activated hyperthermia termination switch design and operation

To realize NIR-triggered hyperthermia in RBC microswimmers as a termination switch, we freshly dissolved ICG in DI water and mixed it with BSA, forming a working solution with ICG (1 mg ml^{-1}) and BSA (60 mg ml^{-1}). Loading and sealing of ICG-BSA were performed using the same process to load DOX molecules. After loading and sealing of ICG-BSA, RBCs were incubated with anti-mouse TER-119 antibody conjugated with biotin for attachment to streptavidin-conjugated bacteria. After incubation, RBCs were centrifuged and resuspended in PBS and mixed with streptavidin-conjugated bacteria for fabrication of RBC microswimmers. Next, RBC microswimmers were loaded in capillary tubes and irradiated under NIR (~0.6 W cm^{-2}), and thermal images were collected using an infrared thermal camera (ETS320, Flir Systems, Wilsonville, OR). Then, samples were recollected in microcentrifuge tubes for fluorescent bacterial viability testing (LIVE/DEAD BacLight Bacterial Viability Kit, Thermo Fisher Scientific, Waltham, MA) and quantification of number of intact RBCs.

Statistical analysis

All quantitative values were presented as means ± SD. All experiments were performed for at least three independent repeats. Mann-Whitney test was used for the statistical analysis, and a *P* value of less than 0.05 was considered statistically significant.

SUPPLEMENTARY MATERIALS

robotics.sciencemag.org/cgi/content/full/3/17/eaar4423/DC1

Fig. S1. Bioengineered *E. coli* MG1655 for biotin attachment peptide expression of the cell membrane.

Fig. S2. Characterization of TER-119 antigen presence on mouse RBCs and binding of biotin-conjugated TER-119 antibodies for streptavidin modification.

Fig. S3. Bioengineered *E. coli* MG1655 attachment to DOX-loaded RBCs.

Fig. S4. Fluorescence microscopy characterization of DOX loading into RBCs.

Fig. S5. Flow cytometry density plots for RBCs without hypotonic isotonic treatment.

Fig. S6. Flow cytometry population selection for RBCs.

Fig. S7. SPION-loaded RBCs are attracted to a permanent magnet.

Fig. S8. Characterization of the loading of citric acid–coated SPIONs into RBCs using EDS.

Fig. S9. Photo of the custom five electromagnetic coils mounted to an inverted optical microscope and used for the magnetic guidance of RBC microswimmers.

Fig. S10. FITC-labeled RBC microswimmers are shown at the entrance of a microchannel.

Fig. S11. Deformation of FITC-labeled RBC microswimmers inside a microchannel with the attached bacterium.

Movie S1. Bacteria-driven RBC microswimmers.

Movie S2. Magnetic steering of bacteria-driven RBC microswimmers.

Movie S3. Passive deformation of RBC microswimmers in microchannels.

Movie S4. Active deformation of an RBC cargo propelled by single bacterium.

REFERENCES AND NOTES

1. R. W. Carlsen, M. Sitti, Bio-hybrid cell-based actuators for microsystems. *Small* **10**, 3831–3851 (2014).
2. M. Sitti, *Mobile Microrobotics* (MIT Press, 2017).
3. M. M. Stanton, S. Sánchez, Pushing bacterial biohybrids to in vivo applications. *Trends Biotechnol.* **35**, 910–913 (2017).
4. Z. Hosseinidoust, B. Mostaghaci, O. Yasa, B.-W. Park, A. V. Singh, M. Sitti, Bioengineered and biohybrid bacteria-based systems for drug delivery. *Adv. Drug Deliv. Rev.* **106** (Pt. A), 27–44 (2016).
5. H. C. Berg, E. coli *in Motion* (Springer Science & Business Media, 2008).
6. H. Mao, P. S. Cremer, M. D. Manson, A sensitive, versatile microfluidic assay for bacterial chemotaxis. *Proc. Natl. Acad. Sci. U.S.A.* **100**, 5449–5454 (2003).
7. B. Behkam, M. Sitti, Bacterial flagella-based propulsion and on/off motion control of microscale objects. *Appl. Phys. Lett.* **90**, 023902 (2007).
8. T. Ahmed, T. S. Shimizu, R. Stocker, Bacterial chemotaxis in linear and nonlinear steady microfluidic gradients. *Nano Lett.* **10**, 3379–3385 (2010).
9. S. J. Park, S.-H. Park, S. Cho, D.-M. Kim, Y. Lee, S. Y. Ko, Y. Hong, H. E. Choy, J.-J. Min, J.-O. Park, S. Park, New paradigm for tumor theranostic methodology using bacteria-based microrobot. *Sci. Rep.* **3**, 3394 (2013).
10. J. Zhuang, R. W. Carlsen, M. Sitti, pH-taxis of biohybrid microsystems. *Sci. Rep.* **5**, 11403 (2015).
11. J. Zhuang, M. Sitti, Chemotaxis of bio-hybrid multiple bacteria-driven microswimmers. *Sci. Rep.* **6**, 32135 (2016).
12. O. Felfoul, M. Mohammadi, S. Taherkhani, D. de Lanauze, Y. Z. Xu, D. Loghin, S. Essa, S. Jancik, D. Houle, M. Lafleur, L. Gaboury, M. Tabrizian, N. Kaou, M. Atkin, T. Vuong, G. Batist, N. Beauchemin, D. Radzioch, S. Martel, Magneto-aerotactic bacteria deliver drug-containing nanoliposomes to tumour hypoxic regions. *Nat. Nanotechnol.* **11**, 941–947 (2016).
13. B. Behkam, M. Sitti, Effect of quantity and configuration of attached bacteria on bacterial propulsion of microbeads. *Appl. Phys. Lett.* **93**, 223901 (2008).
14. A. V. Singh, M. Sitti, Patterned and specific attachment of bacteria on biohybrid bacteria-driven microswimmers. *Adv. Healthc. Mater.* **5**, 2325–2331 (2016).
15. B. Mostaghaci, O. Yasa, J. Zhuang, M. Sitti, Bioadhesive bacterial microswimmers for targeted drug delivery in the urinary and gastrointestinal tracts. *Adv. Sci.* **4**, 1700058 (2017).
16. B.-W. Park, J. Zhuang, O. Yasa, M. Sitti, Multifunctional bacteria-driven microswimmers for targeted active drug delivery. *ACS Nano* **11**, 8910–8923 (2017).
17. S. Taherkhani, M. Mohammadi, J. Daoud, S. Martel, M. Tabrizian, Covalent binding of nanoliposomes to the surface of magnetotactic bacteria for the synthesis of self-propelled therapeutic agents. *ACS Nano* **8**, 5049–5060 (2014).
18. V. D. Nguyen, J.-W. Han, Y. J. Choi, S. Cho, S. Zheng, S. Y. Ko, J.-O. Park, S. Park, Active tumor-therapeutic liposomal bacteriobot combining a drug (paclitaxel)-encapsulated liposome with targeting bacteria (*Salmonella Typhimurium*). *Sens. Actuators B* **224**, 217–224 (2016).
19. A. V. Singh, Z. Hosseinidoust, B.-W. Park, O. Yasa, M. Sitti, Microemulsion-based soft bacteria-driven microswimmers for active cargo delivery. *ACS Nano* **11**, 9759–9769 (2017).
20. K. Higashi, N. Miki, A self-swimming microbial robot using microfabricated nanofibrous hydrogel. *Sens. Actuators B* **202**, 301–306 (2014).
21. M. M. Stanton, B. W. Park, A. Miguel-López, X. Ma, M. Sitti, S. Sánchez, Biohybrid microtube swimmers driven by single captured bacteria. *Small* **13**, 1603679 (2017).
22. R. W. Carlsen, M. R. Edwards, J. Zhuang, C. Pacoret, M. Sitti, Magnetic steering control of multi-cellular bio-hybrid microswimmers. *Lab Chip* **14**, 3850–3859 (2014).

23. D. Li, H. Choi, S. Cho, S. Jeong, Z. Jin, C. Lee, S. Y. Ko, J. O. Park, S. Park, A hybrid actuated microrobot using an electromagnetic field and flagellated bacteria for tumor-targeting therapy. *Biotechnol. Bioeng.* **112**, 1623–1631 (2015).
24. S. Martel, C. C. Tremblay, S. Ngakeng, G. Langlois, Controlled manipulation and actuation of micro-objects with magnetotactic bacteria. *Appl. Phys. Lett.* **89**, 233904 (2006).
25. D. de Lanauze, O. Felfoul, J.-P. Turcot, M. Mohammadi, S. Martel, Three-dimensional remote aggregation and steering of magnetotactic bacteria microrobots for drug delivery applications. *Int. J. Rob. Res.* **33**, 359–374 (2014).
26. C. H. Villa, A. C. Anselmo, S. Mitragotri, V. Muzykantov, Red blood cells: Supercarriers for drugs, biologicals, and nanoparticles and inspiration for advanced delivery systems. *Adv. Drug Deliv. Rev.* **106**, 88–103 (2016).
27. P. Ji, M. Murata-Hori, H. F. Lodish, Formation of mammalian erythrocytes: Chromatin condensation and enucleation. *Trends Cell Biol.* **21**, 409–415 (2011).
28. M. Brähler, R. Georgieva, N. Buske, A. Müller, S. Müller, J. Pinkernelle, U. Teichgräber, A. Voigt, H. Bäumler, Magnetite-loaded carrier erythrocytes as contrast agents for magnetic resonance imaging. *Nano Lett.* **6**, 2505–2509 (2006).
29. C.-M. Hu, R. H. Fang, L. Zhang, Erythrocyte-inspired delivery systems. *Adv. Healthc. Mater.* **1**, 537–547 (2012).
30. J. Shi, L. Kundrat, N. Pishesha, A. Bilate, C. Theile, T. Maruyama, S. K. Dougan, H. L. Ploegh, H. F. Lodish, Engineered red blood cells as carriers for systemic delivery of a wide array of functional probes. *Proc. Natl. Acad. Sci. U.S.A.* **111**, 10131–10136 (2014).
31. P. P. Wibroe, A. C. Anselmo, P. H. Nilsson, A. Sarode, V. Gupta, R. Urbanics, J. Szebeni, A. C. Hunter, S. Mitragotri, T. E. Mollnes, S. M. Moghimi, Bypassing adverse injection reactions to nanoparticles through shape modification and attachment to erythrocytes. *Nat. Nanotechnol.* **12**, 589–594 (2017).
32. Z. Wu, T. Li, J. Li, W. Gao, T. Xu, C. Christianson, W. Gao, M. Galarnyk, Q. He, L. Zhang, J. Wang, Turning erythrocytes into functional micromotors. *ACS Nano* **8**, 12041–12048 (2014).
33. This strain was created by O. Schauer and V. Sourjik, from Max Planck Institute for Terrestrial Microbiology, 35043 Marburg, Germany.
34. M. Delcea, N. Sternberg, A. M. Yashchenok, R. Georgieva, H. Bäumler, H. Möhwald, A. G. Skirtach, Nanoplasmonics for dual-molecule release through nanopores in the membrane of red blood cells. *ACS Nano* **6**, 4169–4180 (2012).
35. I. T. Ivanov, Low pH-induced hemolysis of erythrocytes is related to the entry of the acid into cytosole and oxidative stress on cellular membranes. *Biochim. Biophys. Acta* **1415**, 349–360 (1999).
36. I. F. Tannock, D. Rotin, Acid pH in tumors and its potential for therapeutic exploitation. *Cancer Res.* **49**, 4373–4384 (1989).
37. L. Turner, L. Ping, M. Neubauer, H. C. Berg, Visualizing flagella while tracking bacteria. *Biophys. J.* **111**, 630–639 (2016).
38. N. G. Durmus, H. C. Tekin, S. Guven, K. Sridhar, A. A. Yildiz, G. Calibasi, I. Ghiran, R. W. Davis, L. M. Steinmetz, U. Demirci, Magnetic levitation of single cells. *Proc. Natl. Acad. Sci. U.S.A.* **112**, E3661–E3668 (2015).
39. M. R. Edwards, R. Wright Carlsen, M. Sitti, Near and far-wall effects on the three-dimensional motion of bacteria-driven microbeads. *Appl. Phys. Lett.* **102**, 143701 (2013).
40. Q. Wang, H. Cheng, H. Peng, H. Zhou, P. Y. Li, R. Langer, Non-genetic engineering of cells for drug delivery and cell-based therapy. *Adv. Drug Deliv. Rev.* **91**, 125–140 (2015).
41. Y. Alapan, C. Kim, A. Adhikari, K. E. Gray, E. Gurkan-Cavusoglu, J. A. Little, U. A. Gurkan, Sickle cell disease biochip: A functional red blood cell adhesion assay for monitoring sickle cell disease. *Transl. Res.* **173**, 74–91.e78 (2016).
42. Y. Alapan, Y. Matsuyama, J. A. Little, U. A. Gurkan, Dynamic deformability of sickle red blood cells in microphysiological flow. *Technology* **4**, 71–79 (2016).
43. M. Unal, Y. Alapan, H. Jia, A. G. Varga, K. Angelino, M. Aslan, I. Sayin, C. Han, Y. Jiang, Z. Zhang, U. A. Gurkan, Micro and nano-scale technologies for cell mechanics. *Nanobiomedicine* **1**, 10.5772/59379 (2014).
44. A. Antonelli, M. Magnani, Red blood cells as carriers of iron oxide-based contrast agents for diagnostic applications. *J. Biomed. Nanotechnol.* **10**, 1732–1750 (2014).
45. H. Zhang, Erythrocytes in nanomedicine: An optimal blend of natural and synthetic materials. *Biomater. Sci.* **4**, 1024–1031 (2016).
46. R. Dreyfus, J. Baudry, M. L. Roper, M. Fermigier, H. A. Stone, J. Bibette, Microscopic artificial swimmers. *Nature* **437**, 862–865 (2005).
47. Z. Wu, B. E.-F. de Ávila, A. Martín, C. Christianson, W. Gao, S. K. Thamphiwatana, A. Escarpa, Q. He, L. Zhang, J. Wang, RBC micromotors carrying multiple cargos towards potential theranostic applications. *Nanoscale* **7**, 13680–13686 (2015).
48. M. R. Edwards, R. W. Carlsen, J. Zhuang, M. Sitti, Swimming characterization of *Serratia marcescens* for bio-hybrid micro-robotics. *J. Micro-Bio Rob.* **9**, 47–60 (2014).
49. X. Han, C. Wang, Z. Liu, Red blood cells as smart delivery systems. *Bioconjug. Chem.* (2018).
50. G. Shafirstein, W. Bäumler, L. J. Hennings, E. R. Siegel, R. Friedman, M. A. Moreno, J. Webber, C. Jackson, R. J. Griffin, Indocyanine green enhanced near-infrared laser treatment of murine mammary carcinoma. *Int. J. Cancer* **130**, 1208–1215 (2012).
51. X. Sun, C. Wang, M. Gao, A. Hu, Z. Liu, Remotely controlled red blood cell carriers for cancer targeting and near-infrared light-triggered drug release in combined photothermal–chemotherapy. *Adv. Funct. Mater.* **25**, 2386–2394 (2015).
52. G. Wan, B. Chen, L. Li, D. Wang, S. Shi, T. Zhang, Y. Wang, L. Zhang, Y. Wang, Nanoscaled red blood cells facilitate breast cancer treatment by combining photothermal/photodynamic therapy and chemotherapy. *Biomaterials* **155**, 25–40 (2018).
53. S.-h. Noh, S. H. Moon, T.-H. Shin, Y. Lim, J. Cheon, Recent advances of magneto- thermal capabilities of nanoparticles: From design principles to biomedical applications. *Nano Today* **13**, 61–76 (2017).
54. E. Chambers, S. Mitragotri, Prolonged circulation of large polymeric nanoparticles by non-covalent adsorption on erythrocytes. *J. Control. Release* **100**, 111–119 (2004).
55. A. C. Anselmo, V. Gupta, B. J. Zern, D. Pan, M. Zakrewsky, V. Muzykantov, S. Mitragotri, Delivering nanoparticles to lungs while avoiding liver and spleen through adsorption on red blood cells. *ACS Nano* **7**, 11129–11137 (2013).
56. Y. Alapan, J. A. Little, U. A. Gurkan, Heterogeneous red blood cell adhesion and deformability in sickle cell disease. *Sci. Rep.* **4**, 7173 (2014).
57. Y. Alapan, K. Icoz, U. A. Gurkan, Micro- and nanodevices integrated with biomolecular probes. *Biotechnol. Adv.* **33**, 1727–1743 (2015).
58. Y. Alapan, M. Younesi, O. Akkus, U. A. Gurkan, Anisotropically stiff 3D micropillar niche induces extraordinary cell alignment and elongation. *Adv. Healthc. Mater.* **5**, 1884–1892 (2016).

Acknowledgments: We thank Y. Yu for assistance in the bacteria culture, U. Speck for help in flow cytometry analyses, and N. Krishna-Subbaiah and C. Dayan for help in microfabrication. Y.A. thanks Alexander von Humboldt Foundation for the Humboldt Postdoctoral Research Fellowship. **Funding:** This work was funded by Max Planck Society. **Author contributions:** O.Y. and Y.A. participated in the study design, experimental procedures, data collection, data analysis, and manuscript writing. J.G. and A.F.T. assisted with experimental procedures. O.S. and V.S. designed and created the bacteria strain. M.S. participated in the study design and manuscript writing. **Competing interests:** The authors declare that they have no competing interests. **Data and materials availability:** All data needed to evaluate the conclusions are included in the main text or the Supplementary Materials. Contact M.S. for materials.

Submitted 8 November 2017
Accepted 30 March 2018
Published 25 April 2018
10.1126/scirobotics.aar4423

Citation: Y. Alapan, O. Yasa, O. Schauer, J. Giltinan, A. F. Tabak, V. Sourjik, M. Sitti, Soft erythrocyte-based bacterial microswimmers for cargo delivery. *Sci. Robot.* **3**, eaar4423 (2018).

Science Robotics

Soft erythrocyte-based bacterial microswimmers for cargo delivery

Yunus Alapan, Oncay Yasa, Oliver Schauer, Joshua Giltinan, Ahmet F. Tabak, Victor Sourjik, and Metin Sitti

Sci. Robot. **3** (17), eaar4423. DOI: 10.1126/scirobotics.aar4423

Science Robotics (ISSN 2470-9476) is published by the American Association for the Advancement of Science. 1200 New York Avenue NW, Washington, DC 20005. The title *Science Robotics* is a registered trademark of AAAS.